Chemical Science

ROYAL SOCIETY OF CHEMISTRY

EDGE ARTICLE

View Article Online
View Journal | View Issue

Cite this: *Chem. Sci.*, 2021, **12**, 7858

All publication charges for this article have been paid for by the Royal Society of Chemistry

Received 11th February 2021
Accepted 25th April 2021

DOI: 10.1039/d1sc00861g

rsc.li/chemical-science

Asymmetric synthesis, structures, and chiroptical properties of helical cycloparaphenylenes†

Juntaro Nogami,[a] Yuki Nagashima,[a] Kazunori Miyamoto,[b] Atsuya Muranaka,[c] Masanobu Uchiyama[bc] and Ken Tanaka *[a]

Planar chiral carbon nanorings and nanobelts (CNRs and CNBs), the sidewall segment molecules of chiral-type carbon nanotubes (CNTs), have attracted attention owing to their characteristic chiroptical properties. From the appropriate CNTs, axially or planar chiral CNRs and CNBs have been designed and synthesized, but multiply helical sidewall segments were almost unexplored due to the difficulty in simultaneous control of multiple chiralities. In this article, we have succeeded in the perfectly diastereo- and enantiocontrolled catalytic synthesis of a cycloparaphenylene with four helical and two planar chiralities showing good chiroptical responses as chiral organic molecules. The perfectly stereocontrolled multiply helical structure was confirmed by a single-crystal X-ray diffraction analysis. The experimental and theoretical studies established the importance of the highly symmetric multiply helical structure in the cylindrical axis in obtaining good chiroptical responses.

Introduction

Carbon nanorings[1] and nanobelts[2] (CNRs and CNBs), the sidewall segment molecules of carbon nanotubes (CNTs), have attracted attention for their unique characters, derived from their curved and strained structures.[3] Recently, chiral CNRs and CNBs have also attracted attention owing to their characteristic chiroptical properties, such as enhanced responses in electronic circular dichroism (ECD) and circularly polarized luminescence (CPL).[4] So far, the following chiral CNRs and CNBs embedding configurationally stable non-centro chirality have been designed by cutting out the appropriate sidewall segments from the CNTs, and their bottom-up syntheses were accomplished. For example, Isobe designed planar chiral CNRs, as represented by CNR **a**[5] (Fig. 1A), by cutting out the configurationally stable arene units,[4b,5,6] and Miao/Chi designed CNBs possessing doubly stranded planar chiral arene units.[2c] Itami,[7] Swager,[8] Isobe,[9] Müllen,[10] and Mazaki[11] designed axially chiral CNRs, as represented by CNR **b**,[7a] by cutting out the configurationally stable biaryl units (Fig. 1B). Our research group designed planar chiral cyclophenylenes (CPs), as represented by CP **c**,[12] by the introduction of asymmetric substituents into the achiral CPs (Fig. 1C). Although some complicated chiral CNRs[9d] and CNBs[2c] are accompanied by [4]helicene units on their peripheries as subsidiary components, CNT segments with configurationally stable [*n*]helicene units ($n \geq 5$) have not been reported. Recently, Segawa and Itami disclosed the design and the strain energy of helicene-containing CNBs, but the synthesis of these theoretically predicted molecules has not been achieved.[13] Furthermore, no studies have been reported on the chiroptical properties caused by the helical chirality of the chiral CNRs and CNBs. Concerning the synthesis, chiral CNRs were often obtained as mixtures of stereoisomers because non-enantioselective aryl–aryl couplings were used.[1] Although the use of chiral cholesterol stearate could afford CNR **a** with 17% ee,[5] and the kinetically controlled Scholl reaction and thermal epimerization could afford the planar chiral CNB[2c] and CNR **b**,[7a] respectively, as a single diastereomer, their highly enantioselective syntheses have not been achieved. On the other hand, our research group synthesized CP **c**[12] with 98% ee by the rhodium-catalyzed intramolecular alkyne cyclotrimerization,[14] which demonstrated the high utility of alkyne cyclotrimerization for the enantioselective synthesis of chiral CNRs and CNBs.[15,16]

In this article, we report the perfectly diastereo- and enantiocontrolled catalytic synthesis (>99% ee) and good chiroptical responses of multiply helical cycloparaphenylene (CPP) (*Sp*,*Sp*)-(*M*,*M*,*M*,*M*)-**1a** with four helical and two planar chiralities, which is designed by cutting out configurationally stable helical units from the armchair-type CNT (Fig. 1D). Experimental and theoretical studies revealed the importance of the highly

[a]*Department of Chemical Science and Engineering, Tokyo Institute of Technology, O-okayama, Meguro-ku, Tokyo 152-8550, Japan. E-mail: ktanaka@apc.titech.ac.jp*

[b]*Advanced Elements Chemistry Laboratory, Cluster for Pioneering Research (CPR), RIKEN, 2-1 Hirosawa, Wako, Saitama351-0198, Japan*

[c]*Graduate School of Pharmaceutical Sciences, The University of Tokyo, 7-3-1 Hongo, Bunkyo-ku, Tokyo 113-0033, Japan*

† Electronic supplementary information (ESI) available. CCDC 2050855. For ESI and crystallographic data in CIF or other electronic format see DOI: 10.1039/d1sc00861g

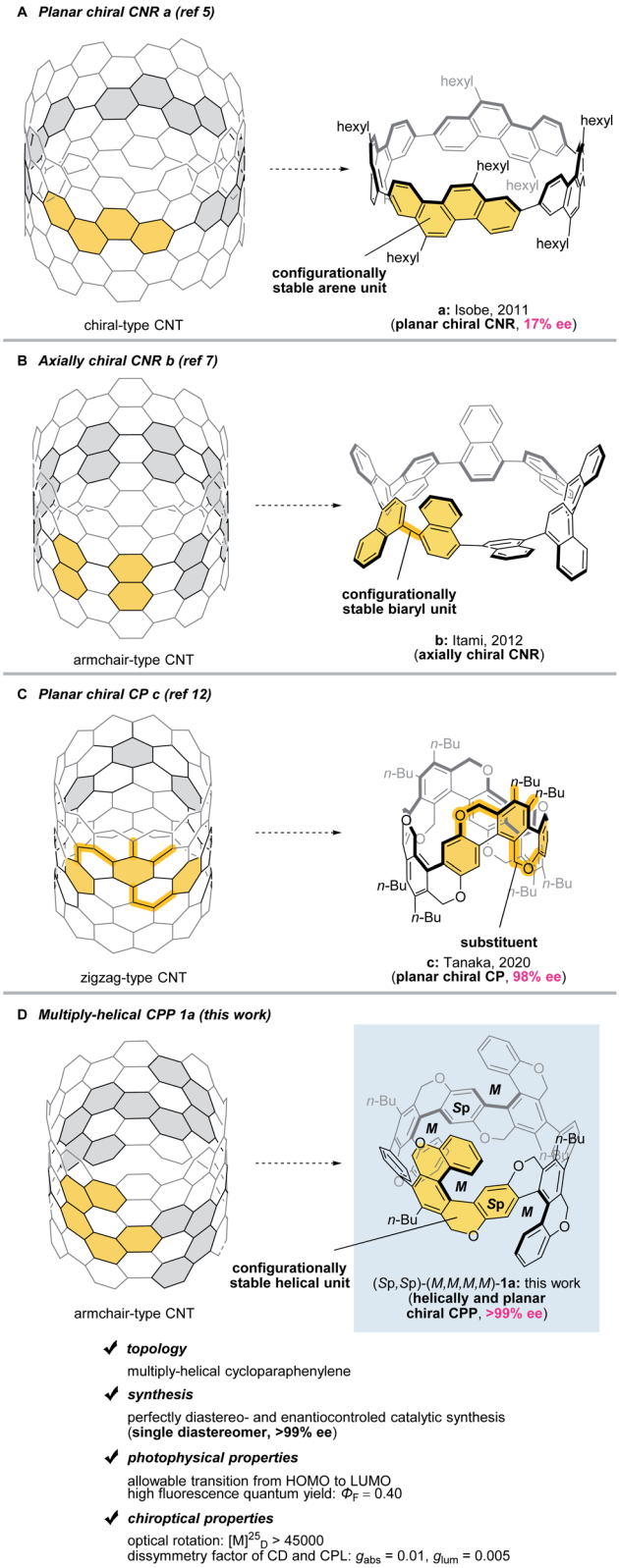

Fig. 1 Chiral sidewall segment molecules of CNTs. (A) Planar chiral CNR **a**.[5] (B) Axially chiral CNR **b**.[7] (C) Planar chiral CP **c**.[12] (D) Multiply-helical CPP **1a** (this work).

symmetric multiply helical structure in the cylindrical axis to realize the observed good chiroptical responses as chiral organic molecules.

Results and discussion

Diastereo- and enantioselective synthesis

The synthetic route to [12]CPP **1b** as well as [8]CPP **1a** is shown in Fig. 2. The palladium-catalyzed Sonogashira-coupling of known diiodide **2** and terminal alkyne **3** afforded tetrayne **4**, and the subsequent acid hydrolysis afforded bisphenol **5** in 82% yield from **2**. Bispropargylation of **5** with dibromide **6** generated dodecayne **7a** and octadecayne **7b** in 12% and 6% yields, respectively. Pleasingly, the intramolecular four sequential cyclotrimerizations of **7a** proceeded at 40 °C by using a cationic rhodium(I)/(*S*)-H_8-BINAP catalyst to give [8]CPP (*Sp*,*Sp*)-(*M*,*M*,*M*,*M*)-(−)-**1a** with four helical and two planar chiralities as a single diastereomer with 96% ee and 36% yield, although the room temperature reaction was sluggish. Screening of axially chiral biaryl bisphosphine ligands revealed that decreasing the dihedral angle linearly increases the ee value [dihedral angle: H_8-BINAP (75°) > BINAP (74°) > Segphos (66°),[17] ee value: H_8-BINAP < BINAP < Segphos] and the use of (*S*)-Segphos generates **1a** with >99% ee and 40% yield, which corresponds to 80% yield in each cyclotrimerization. As with **1a**, the intramolecular six sequential cyclotrimerizations of **7b** also proceeded at 40 °C and the use of (*S*)-Segphos generated (*Sp*,*Sp*,*Rp*)-(*M*,*M*,*M*,*M*,*P*,*P*)-(−)-**1b** with the highest ee value of 62%. Although a trace amount (*ca.* 5%) of another diastereomer [presumably (*Sp*,*Sp*,*Sp*)-(*M*,*M*,*M*,*M*,*M*,*M*)-**1b**] was generated, this diastereomer could not be isolated in a pure form. This ee value was lower than that of **1a**, but the yield was improved to 59%, which corresponds to 92% yield in each cyclotrimerization. In these reactions, complex mixtures of by-products were generated presumably as a result of the competitive intermolecular side reactions.

Structural analyses

(*Sp*,*Sp*)-(*M*,*M*,*M*,*M*)-**1a** gave a relatively simple ^{1}H NMR spectrum due to its highly symmetrical structure (D_2 symmetry in solution) (Fig. 3A). Three singlet peaks are observed in the aromatic region, one of which (pink) corresponds to the S-shaped helicene-core and the other two (red and blue) to the *p*-phenylene unit. If the *p*-phenylene rings rotate smoothly on the NMR time scale, red and blue hydrogens should be equivalent and afford one singlet peak. The obtained ^{1}H NMR spectrum indicates that the rotation of *p*-phenylene units is suppressed, which results in the inner proton (blue) and the outer proton (red) placed in different magnetic environments affording two singlet peaks.

On the other hand, compound **1b** gave a more complicated ^{1}H NMR spectrum shown in Fig. 3B. There are two possible diastereomers, (*Sp*,*Sp*,*Sp*)-(*M*,*M*,*M*,*M*,*M*,*M*)-**1b** and (*Sp*,*Sp*,*Rp*)-(*M*,*M*,*M*,*M*,*P*,*P*)-**1b**, of which (*Sp*,*Sp*,*Sp*)-(*M*,*M*,*M*,*M*,*M*,*M*)-isomer (D_3 symmetry) should have the same number of ^{1}H NMR peaks as those of (*Sp*,*Sp*)-(*M*,*M*,*M*,*M*)-**1a**. However, the observed ^{1}H

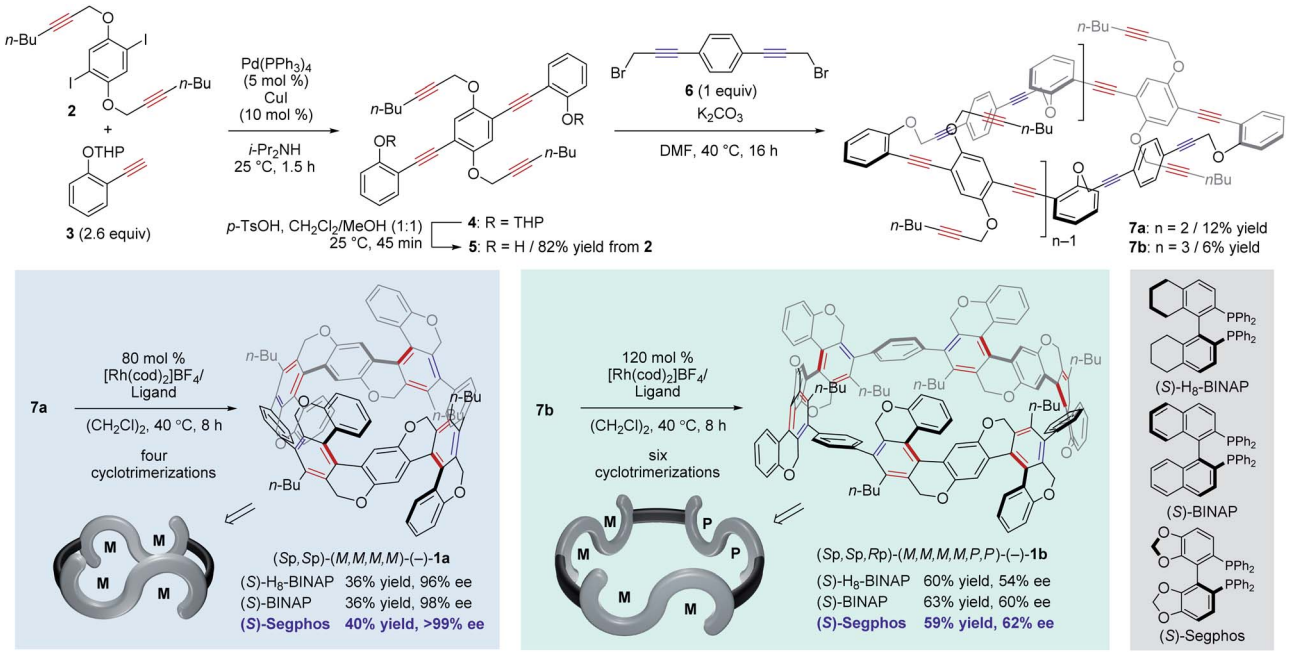

Fig. 2 Rhodium-catalyzed diastereo- and enantioselective synthesis of CPPs with helical and planar chiralities. THP = 2-tetrahydropyranyl. *p*-TsOH = *p*-toluenesulfonic acid. DMF = *N*,*N*-dimethylformamide. cod = 1,5-cyclooctadiene. [a] Calculated dihedral angles of Ru/ligand complexes shown in ref. 17.

NMR has more peaks, suggesting that **1b** has non-uniform multiple chiralities. Six singlet peaks in the aromatic region (6.6–8.0 ppm) and 12 doublet peaks in the methylene region (4.5–5.2 ppm) were observed, which match the number of ^{1}H NMR peaks of the C_2-symmetrical (*Sp*,*Sp*,*Rp*)-(*M*,*M*,*M*,*M*,*P*,*P*)-isomer. In the ^{13}C NMR spectrum, the six alkyne peaks (75–90 ppm) of precursor **1b** disappeared, and the same number of peaks appeared as expected in the (*Sp*,*Sp*,*Rp*)-(*M*,*M*,*M*,*M*,*P*,*P*)-isomer. (51 peaks in the aromatic region, 6 peaks in the methylene region, and 12 peaks in the *n*-Bu region). 2D NMR (NOESY,

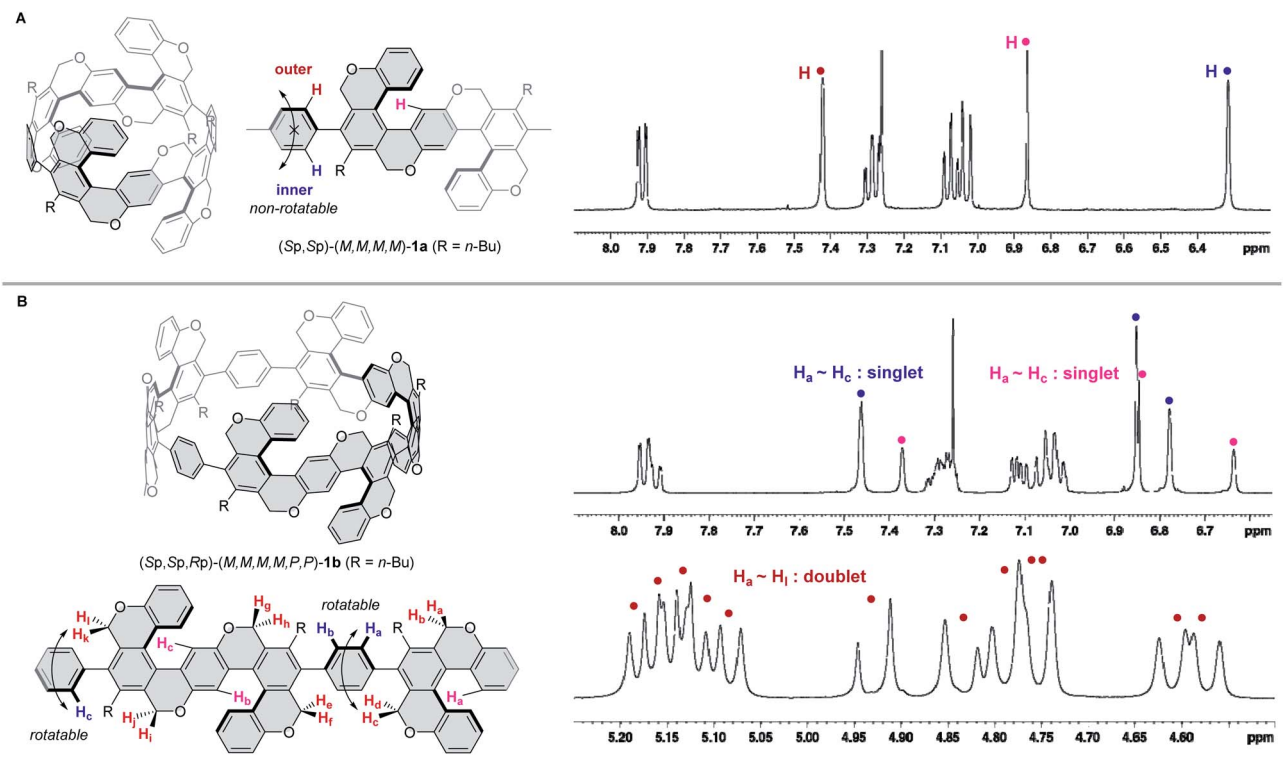

Fig. 3 ^{1}H NMR spectra of (*Sp*,*Sp*)-(*M*,*M*,*M*,*M*)-**1a** (A) and (*Sp*,*Sp*,*Rp*)-(*M*,*M*,*M*,*M*,*P*,*P*)-**1b** (B).

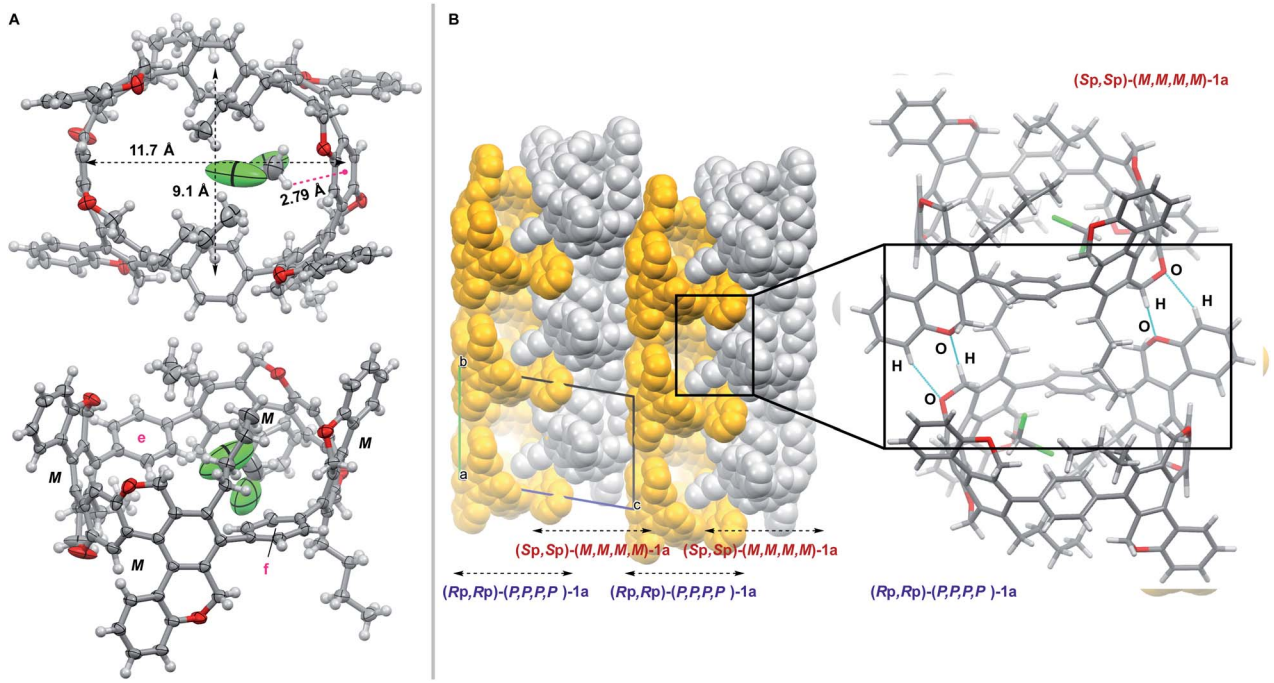

Fig. 4 Single-crystal X-ray diffraction analysis of (±)-**1a**. (A) ORTEP drawings (top: top view, bottom: side view) showing thermal ellipsoids at 50% probability. (B) Packing structures (left) and bimolecular interactions (right).

COSY, HMBC, and HSQC) were also recorded to increase the reliability of the structure, and all the above NMR analysis data confirm the formation of (*S*p,*S*p,*R*p)-(*M*,*M*,*M*,*M*,*P*,*P*)-**1b**.

A single crystal of (±)-**1a**, in which one molecule of CH_2Cl_2 is subsumed inside presumably due to the strong CH···π interaction (2.79 Å), was obtained by slow diffusion of *n*-hexane into a CH_2Cl_2 solution of (±)-**1a**, which was synthesized by the cyclotrimerization of **7a** using (±)-BINAP. Its crystal structure was determined by a single-crystal X-ray diffraction analysis (Fig. 4). All four helical units have the same chirality, and this CPP has an ellipse shape (major diameter = 11.7 Å, minor diameter = 9.1 Å) with two greatly curved S-shaped helical units, which is in sharp contrast to the circle shape of unsubstituted [8]CPP.[3a] The conformation of the two *p*-phenylene units **e** and **f**, sandwiched between the S-shaped helical units, is not parallel but a V-shaped conformation (Fig. 4A). For the packing structure, each of the *P*-isomer and the *M*-isomer forms an independent columnar structure, and they are arranged alternately with C–H···O interactions between adjacent columns (Fig. 4B). Although we failed to obtain chiral single crystals of **1a** and **1b**, the absolute configurations of (*S*p,*S*p)-(*M*,*M*,*M*,*M*)-(−)-**1a** and (*S*p,*S*p,*R*p)-(*M*,*M*,*M*,*M*,*P*,*P*)-(−)-**1b** could be confirmed by comparison of the experimental ECD spectra of (−)-**1a** and (−)-**1b**, and theoretical ECD spectra of (*S*p,*S*p)-(*M*,*M*,*M*,*M*)-Me_4-**1a** and (*S*p,*S*p,*R*p)-(*M*,*M*,*M*,*M*,*P*,*P*)-Me_6-**1b** (Fig. S10–S13†).

The stability of chiralities in **1a** and **1b** was examined by heating the solution of (*S*p,*S*p)-(*M*,*M*,*M*,*M*)-**1a** and (*S*p,*S*p,*R*p)-(*M*,*M*,*M*,*M*,*P*,*P*)-**1b**. No epimerization and racemization was observed for (*S*p,*S*p)-(*M*,*M*,*M*,*M*)-**1a** even at 110 °C in toluene for 16 hours due to its stable planar and helical chiralities. In contrast, the racemization of (*S*p,*S*p,*R*p)-(*M*,*M*,*M*,*M*,*P*,*P*)-**1b** gradually proceeded even at 60 °C in $(CH_2Cl)_2$ (Fig. 5). The formation of a trace amount of an epimerization product [presumably (*S*p,*S*p,*S*p)-(*M*,*M*,*M*,*M*,*M*,*M*)-**1b**, diastereomeric ratio = *ca.* 30 : 1] was detected at 80 °C in $(CH_2Cl)_2$ for 19 hours. The difference in the stability of chirality between **1a** and **1b** depends on the ring strain. The strain energy of **1b** (ΔH = −43.9 kcal mol^{-1}) is smaller than that of **1a** (ΔH = −62.9 kcal mol^{-1}) (Fig. S7 and S8†), which results in the lower chiral stability of **1b** than **1a**. Concerning the thermodynamic stabilities of two possible diastereomers (*S*p,*S*p,*S*p)-(*M*,*M*,*M*,*M*,*M*,*M*)-**1b** and (*S*p,*S*p,*R*p)-(*M*,*M*,*M*,*M*,*P*,*P*)-**1b**, DFT calculation revealed that (*S*p,*S*p,*R*p)-(*M*,*M*,*M*,*M*,*P*,*P*)-**1b** was slightly more stable than (*S*p,*S*p,*S*p)-(*M*,*M*,*M*,*M*,*M*,*M*)-**1b** (ΔG = 0.55 kcal mol^{-1}). (*S*p,*S*p,*R*p)-(*M*,*M*,*M*,*M*,*P*,*P*)-**1b** was generated at

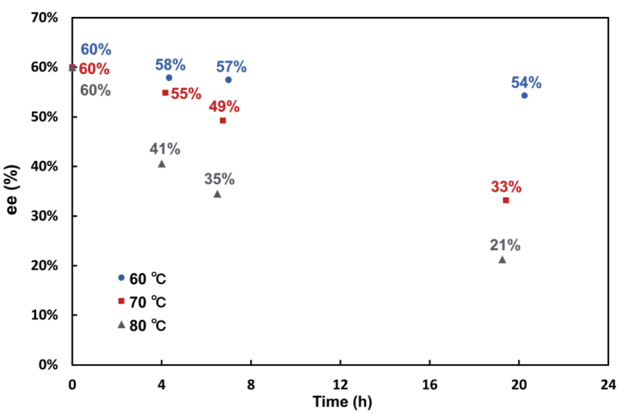

Fig. 5 Stability of the chiralities of (*S*p,*S*p,*R*p)-(*M*,*M*,*M*,*M*,*P*,*P*)-**1b** in $(CH_2Cl)_2$.

a higher ratio (>12 : 1) than its thermodynamic stability (calculated ratio = 2.4 : 1) because no epimerization proceeds at the reaction temperature (40 °C), and the cyclotrimerization reaction proceeds with kinetic control. The fact that the diastereomer of **1b**, in which three planar chiralities are not identical, was kinetically predominant is consistent with the previously reported triply twisted Möbius molecules.[18] On the other hand, (*S*p,*S*p,*R*p)-(*M*,*M*,*M*,*M*,*P*,*P*)-**1b** was obtained from **7b** with significantly lower ee value (6 2% ee) than (*S*p,*S*p)-(*M*,*M*,*M*,*M*)-**1a** (>99% ee) derived from **7a**. Since **1b** was

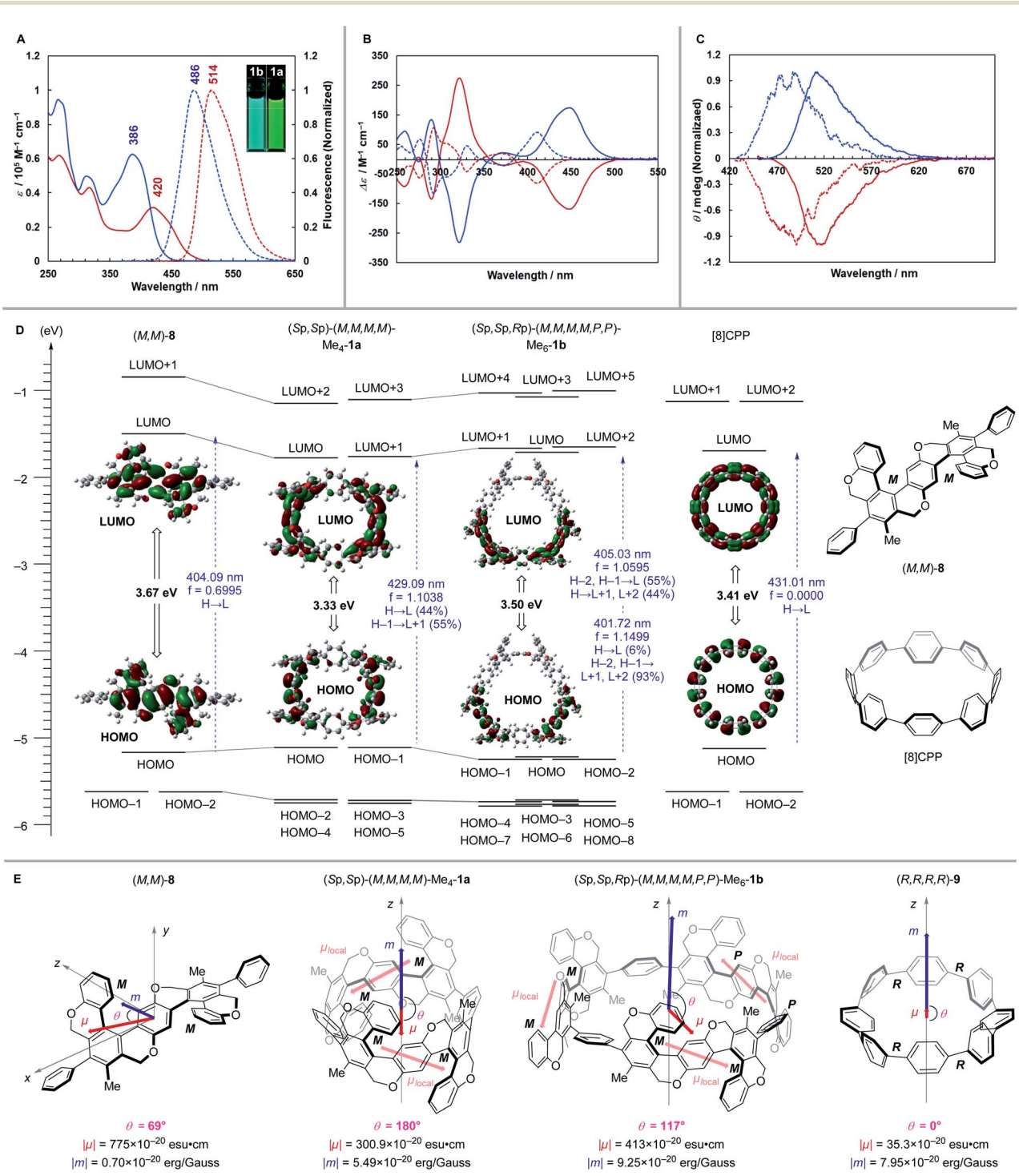

Fig. 6 Photophysical and chiroptical properties. (A) Absorption (solid line) and fluorescence (broken line) spectra of [(*S*p,*S*p)-(*M*,*M*,*M*,*M*)-**1a** (red) and (*S*p,*S*p,*R*p)-(*M*,*M*,*M*,*M*,*P*,*P*)-**1b** (blue) in CH_2Cl_2 at 25 °C. ECD (B) and CPL (C) spectra of **1a** (solid line) [(*S*p,*S*p)-(*M*,*M*,*M*,*M*)-**1a**: red, (*R*p,*R*p)-(*P*,*P*,*P*,*P*)-**1a**: blue] and **1b** (broken line) [(*S*p,*S*p,*R*p)-(*M*,*M*,*M*,*M*,*P*,*P*)-**1b**: red, (*R*p,*R*p,*S*p)-(*P*,*P*,*P*,*P*,*M*,*M*)-**1b**: blue] in CH_2Cl_2 at 25 °C. (D) Calculating the energy diagrams of (*M*,*M*)-**8**, (*S*p,*S*p)-(*M*,*M*,*M*,*M*)-Me_4-**1a**, (*S*p,*S*p,*R*p)-(*M*,*M*,*M*,*M*,*P*,*P*)-Me_6-**1b**, and [8]CPP. (E) Calculating the transition dipole moments of (*M*,*M*)-**8**, (*S*p,*S*p)-(*M*,*M*,*M*,*M*)-Me_4-**1a**, (*S*p,*S*p,*R*p)-(*M*,*M*,*M*,*M*,*P*,*P*)-Me_6-**1b**, and (*R*,*R*,*R*,*R*)-**9**.

configurationally stable at the reaction temperature of 40 °C and perfect enantioselectivity (>99% ee) was observed in our previously reported enantioselective synthesis of a double [6] helicene-like molecule by the rhodium-catalyzed intramolecular cyclotrimerization of a triyne,[19] the racemization process might be included during the sequential cyclotrimerization of **7b**.

Photophysical and chiroptical properties

Absorption and fluorescence spectra of (*S*p,*S*p)-(*M*,*M*,*M*,*M*)-**1a** and (*S*p,*S*p,*R*p)-(*M*,*M*,*M*,*M*,*P*,*P*)-**1b** are shown in Fig. 6A, and the data are summarized in Table 1. **1a** and **1b** showed absorption up to the nearly visible region with absorption maxima at 420 nm and 386 nm, respectively. These wavelengths are much longer than the maximum absorption wavelengths of unsubstituted CPPs, which have absorption maxima at around 340 nm regardless of the ring-size. **1a** and **1b** showed yellow green and blue green fluorescence and their fluorescence maxima are 514 nm and 486 nm, respectively, and thus fluorescence peak-shifts in comparison with unsubstituted CPPs are moderate ([8]CPP: 533 nm [12]CPP: 450 nm).[3a] Fluorescence quantum yields of **1a** and **1b** are 40% and 48%, respectively, and the yield of **1a** is notably higher than that of [8]CPP ($\Phi_F = 10\%$).[3a] These optical properties may be derived from the S-shaped helical structures because those are close to the values of not the CPPs but our previously reported S-shaped double [6]helicene-like molecule ($\lambda_{abs} = 361$ nm, $\lambda_{lum} = 466$ nm, $\Phi_F = 48\%$).[20]

To understand the above optical properties, DFT and TDDFT calculations of (*S*p,*S*p)-(*M*,*M*,*M*,*M*)-Me_4-**1a** and (*S*p,*S*p,*R*p)-(*M*,*M*,*M*,*M*,*P*,*P*)-Me_6-**1b** were performed using Gaussian 16 at the B3LYP/6-31G(d) level of theory (Fig. 6D). HOMO/HOMO–1 and LUMO/LUMO+1 of Me_4-**1a** pseudodegenerate, and HOMO–2/HOMO–1/HOMO and LUMO/LUMO+1/LUMO+2 of Me_6-**1b** also pseudodegenerate. These pseudodegenerate molecular orbitals show good agreement with energy levels and orbital shapes of the partial structure, S-shaped double helicene-like molecule (*M*,*M*)-**8**. The *p*-phenylene spacer hardly contributes to the electronic structure of HOMO and LUMO (Fig. 6D, S3, and S4†), which diminishes the CPP character. The HOMO → LUMO transitions in Me_4-**1a** and Me_6-**1b** are allowable, which are different from the symmetry-forbidden HOMO → LUMO transitions of the CPPs. These transitions have large oscillator strengths like **8** and correspond to the longest wavelength absorption bands. However, as with the CPPs, the HOMO–LUMO energy gap decreases in this order, **8** (3.67 eV) > Me_6-**1b** (3.50 eV) > Me_4-**1a** (3.33 eV), as the bend increases as shown in Fig. S7 and S8,† which is consistent with the experimental fact that **1a** has an absorption maximum in the longer wavelength region than **1b**.

Next, chiroptical properties of (*S*p,*S*p)-(*M*,*M*,*M*,*M*)-**1a** and (*S*p,*S*p,*R*p)-(*M*,*M*,*M*,*M*,*P*,*P*)-**1b** were also measured (Fig. 6B and C), and the data are summarized in Table 2. The molar optical rotation, $[M]_D^{25}$, is extremely large for both **1a** and **1b**, especially **1a** showed a value exceeding 45 000 degree, which is as large as that of [11]helicene.[21,22] The existence of multiple identical helicities in the molecule may induce this large optical rotation value. Their ECD and CPL spectra exhibited mirror images corresponding to the enantiomers. The dissymmetry factor of ECD (g_{abs}) and CPL (g_{lum}) of **1a** are 0.0095 and 0.0049, respectively, which are twice as large as those of our previously reported planar chiral CP **c**,[12] although these values are smaller than those of cyclochrysenylene[4a] and cycloanthracene.[4b] However, the g_{abs} and g_{lum} values of **1b**, possessing mixed *P*/*M* chirality, are 0.0027 and 0.0017, respectively, which are smaller than those of **1a**.

The structure–chiroptical property relationship was also examined by TDDFT calculations (Fig. 6E). The g_{abs} value is expressed by the following equation, in which μ, m, and θ are the electric transition dipole moment, magnetic transition dipole moment, and the angle between μ and m, respectively.

$$g_{abs} = \frac{\Delta\varepsilon(\lambda)}{\varepsilon(\lambda)} = \frac{4R}{D} = \frac{4|\mu||m|\cos\theta}{|\mu|^2 + |m|^2}$$

From the above equation, it is necessary to reach $\theta = 0°$ or 180° ($\cos\theta = \pm 1$) and $|m|/|\mu| = 1$ to realize a high g_{abs} value.

Table 1 Photophysical data of **1a** and **1b**

Compound	$\lambda_{abs,max}$[b] (nm)	ε_{max}[c] (M^{-1} cm^{-1})	$\lambda_{em,max}$[d] (nm)	Φ_F[e]
(*S*p,*S*p)-(*M*,*M*,*M*,*M*)-**1a**[a]	420	31 300	514	0.40
(*S*p,*S*p,*R*p)-(*M*,*M*,*M*,*M*,*P*,*P*)-**1b**[a]	386	62 500	486	0.48

[a] In CH_2Cl_2 (1.0×10^{-5} M) at 25 °C. [b] $\lambda_{abs,max}$: longest wavelength absorption maximum. [c] ε_{max}: molar extinction coefficient. [d] $\lambda_{em,max}$: fluorescence maximum. [e] Φ_F: fluorescence quantum yield. The excitation wavelengths of **1a** and **1b** are 420 nm and 390 nm, respectively.

Table 2 Chiroptical data of **1a** and **1b**

Compound	$[\alpha]_D^{25}$[d]	$[M]_D^{25}$[e]	g_{abs}[f]/10^{-3} (wavelength)	g_{lum}[g]/10^{-3} (wavelength)
(*S*p,*S*p)-(*M*,*M*,*M*,*M*)-**1a** (>99% ee)[a]	−3357°	−45 700°	−9.48 (461)	−4.92 (512)
(*R*p,*R*p)-(*P*,*P*,*P*,*P*)-**1a** (>99% ee)[b]	—	—	+9.58 (462)	+4.95 (512)
(*S*p,*S*p,*R*p)-(*M*,*M*,*M*,*M*,*P*,*P*)-**1b** (62% ee)[a]	−466°[c]	−9520°[c]	−2.74 (422)[c]	−1.67 (490)[c]
(*R*p,*R*p,*S*p)-(*P*,*P*,*P*,*P*,*M*,*M*)-**1b** (62% ee)[b]	—	—	+2.90 (424)[c]	+1.97 (488)[c]

[a] In CH_2Cl_2 (1.0×10^{-5} M) at 25 °C. [b] In CH_2Cl_2 (1.1×10^{-5} M) at 25 °C. [c] Values are calculated as 100% ee. [d] $[\alpha]_D^{25}$: optical rotation. [e] $[M]_D^{25}$: molar optical rotation ($= M[\alpha]_D^{25}/100$). [f] g_{abs}: CD dissymmetry factor. [g] g_{lum}: CPL dissymmetry factor.

Thus, it is important to align μ and m in parallel and enhance $|m|$, while conventional chiral organic molecules have negligible $|m|$. To date, ideal topologies have been found in planar chiral cylindrical carbon nanohoops[4,5] and highly symmetric multihelicenes.[23,24] The TDDFT calculation of partial structure (*M*,*M*)-**8** revealed that undesirable large μ is generated in the direction perpendicular to the C_2 axis in the $S_0 \rightarrow S_1$ transition, and θ is also undesirable (69°). On the other hand, in the $S_0 \rightarrow S_1$ transition of (*S*p,*S*p)-(*M*,*M*,*M*,*M*)-Me_4-**1a**, ideal small $|\mu|$ and large $|m|$ as well as ideal θ (180°) are generated. Thus, the symmetrical arrangement of S-shaped helical units improves the g_{abs} value.

According to the decomposition analysis by Isobe,[6d] μ of (*S*p,*S*p)-(*M*,*M*,*M*,*M*)-Me_4-**1a** can be divided into two μ_{local} of two S-shaped helical units, and μ_{local} can be expressed schematically as the μ of (*M*,*M*)-**8**. The symmetrical arrangement of two μ_{local} in the *z*-axis results in the ideal θ value (180°). However, in (*S*p,*S*p,*R*p)-(*M*,*M*,*M*,*M*,*P*,*P*)-Me_6-**1b**, θ becomes 117° because three μ_{local} lose symmetry in the *z*-axis. From the above discussion, the hypothetical molecule (*R*,*R*,*R*,*R*)-**9**, corresponding to the twisted [8]CPP unit of (*S*p,*S*p)-(*M*,*M*,*M*,*M*)-Me_4-**1a**, would have a small μ value while maintaining the ideal θ value. Indeed, the TDDFT calculation of **9** revealed that the parallel arrangement of μ and m is maintained, and $|m|/|\mu|$ is significantly larger than that of (*S*p,*S*p)-(*M*,*M*,*M*,*M*)-Me_4-**1a**. Thus, it is expected that a molecule with excellent chiroptical responses can be created if a method for inducing and stabilizing the multiply helical CPP structure with appropriate dihedral angles like (*R*,*R*,*R*,*R*)-**9** can be developed.

Conclusions

In conclusion, we have achieved the perfectly diastereo- and enantiocontrolled catalytic synthesis of cycloparaphenylene (CPP) **1a** containing two double [5]helicene-like molecules, the structure of which was confirmed by a single-crystal X-ray diffraction analysis. A CPP containing three double [5] helicene-like molecules has also been synthesized, although the ee value was moderate. The stability of chiralities in **1a** and **1b** were examined by heating the solution of **1a** and **1b**, which revealed that no epimerization and racemization were observed for **1a** even at 110 °C, whereas the racemization of **1b** gradually proceeded even at 60 °C. CPP **1a** showed good chiroptical responses, such as the large molar optical rotation ($[M]_D^{25}$ = 45 700°), and the dissymmetry factors of ECD (g_{abs} = 0.0095) and CPL (g_{lum} = 0.0049). The experimental and theoretical studies established the importance of the highly symmetric multiply helical structure in the cylindrical axis in obtaining good chiroptical responses. Finally, we proposed that the hypothetical multiply helical molecule (*R*,*R*,*R*,*R*)-**9** would show excellent chiroptical responses hence the method for inducing and stabilizing this multiply helical CPP structure with appropriate dihedral angles can be developed.

Author contributions

J. N. designed the project and carried out the experimental work. J. N. also carried out computational studies and wrote a draft under the guidance of Y. N. K. M. performed the X-ray crystal structure analysis and A.M. performed CPL measurements. Y. N., A. M., and M. U. analyzed and discussed the experimental work and computational studies. K. T. designed and directed the project, and wrote the manuscript.

Conflicts of interest

There are no conflicts to declare.

Acknowledgements

This research was supported partly by Grants-in-Aid for Scientific Research (No. JP19H00893 to K. T. and No. 17H06173 to M. U.) from JSPS (Japan) and CREST (No. JPMJCR19R2 to M. U.) from JST (Japan). We thank Takasago International Corporation for the gift of Segphos and H_8-BINAP, and Umicore for their generous support in supplying the palladium and rhodium complexes. A generous allotment of computational resources from TSUBAME (Tokyo Institute of Technology) is gratefully acknowledged.

Notes and references

1 For reviews, see: (*a*) M. A. Majewski and M. Stępień, *Angew. Chem., Int. Ed.*, 2019, **58**, 86; (*b*) Y. Segawa, A. Yagi, K. Matsui and K. Itami, *Angew. Chem., Int. Ed.*, 2016, **55**, 5136; (*c*) D. Eisenberg, R. Shenhar and M. Rabinovitz, *Chem. Soc. Rev.*, 2010, **39**, 2879. For pioneering works, see: ; (*d*) R. Jasti, J. Bhattacharjee, J. B. Neaton and C. R. Bertozzi, *J. Am. Chem. Soc.*, 2008, **130**, 17646; (*e*) H. Takaba, H. Omachi, Y. Yamamoto, J. Bouffard and K. Itami, *Angew. Chem., Int. Ed.*, 2009, **48**, 6112; (*f*) S. Yamago, Y. Watanabe and T. Iwamoto, *Angew. Chem., Int. Ed.*, 2010, **49**, 757.

2 (*a*) G. Povie, Y. Segawa, T. Nishihara, Y. Miyauchi and K. Itami, *Science*, 2017, **356**, 172; (*b*) G. Povie, Y. Segawa, T. Nishihara, Y. Miyauchi and K. Itami, *J. Am. Chem. Soc.*, 2018, **140**, 10054; (*c*) K. Y. Cheung, S. Gui, C. Deng, H. Liang, Z. Xia, Z. Liu, L. Chi and Q. Miao, *Chem*, 2019, **5**, 838; (*d*) K. Y. Cheung, K. Watanabe, Y. Segawa and K. Itami, *Nat. Chem.*, 2021, **13**, 255; (*e*) C. Chi, Y. Han, S. Dong, J. Shao and W. Fan, *Angew. Chem., Int. Ed.*, 2020, **60**, 2658; (*f*) Z. Xia, S. H. Pun, H. Chen and Q. Miao, *Angew. Chem., Int. Ed.*, 2021, **60**, 10311.

3 For reviews, see: (*a*) K. Y. Cheung, Y. Segawa and K. Itami, *Chem.–Eur. J.*, 2020, **26**, 14791; (*b*) H. Chen, S. Gui, Y. Zhang, Z. Liu and Q. Miao, *CCS Chem.*, 2020, **2**, 613; (*c*) H. Chen and Q. Miao, *J. Phys. Org. Chem.*, 2020, **33**, 1; (*d*) Y. Xu and M. von Delius, *Angew. Chem., Int. Ed.*, 2020, **59**, 559; (*e*) E. R. Darzi and R. Jasti, *Chem. Soc. Rev.*, 2015, **44**, 6401.

4 (*a*) S. Sato, A. Yoshii, S. Takahashi, S. Furumi, M. Takeuchi and H. Isobe, *Proc. Natl. Acad. Sci. U. S. A.*, 2017, **114**, 13097; (*b*) J. Wang, G. Zhuang, M. Chen, D. Lu, Z. Li, Q. Huang, H. Jia, S. Cui, X. Shao, S. Yang and P. Du, *Angew. Chem., Int. Ed.*, 2020, **59**, 1619.

5 S. Hitosugi, W. Nakanishi, T. Yamasaki and H. Isobe, *Nat. Commun.*, 2011, **2**, 492.
6 (*a*) S. Hitosugi, T. Yamasaki and H. Isobe, *J. Am. Chem. Soc.*, 2012, **134**, 12442; (*b*) T. Matsuno, S. Kamata, S. Hitosugi and H. Isobe, *Chem. Sci.*, 2013, **4**, 3179; (*c*) Z. Sun, P. Sarkar, T. Suenaga, S. Sato and H. Isobe, *Angew. Chem., Int. Ed.*, 2015, **54**, 12800; (*d*) K. Kogashi, T. Matsuno, S. Sato and H. Isobe, *Angew. Chem., Int. Ed.*, 2019, **58**, 7385.
7 (*a*) A. Yagi, Y. Segawa and K. Itami, *J. Am. Chem. Soc.*, 2012, **134**, 2962; (*b*) K. Okada, A. Yagi, Y. Segawa and K. Itami, *Chem. Sci.*, 2016, **8**, 661.
8 J. M. Batson and T. M. Swager, *Synlett*, 2013, **24**, 2545.
9 (*a*) K. Ikemoto, S. Sato and H. Isobe, *Chem. Lett.*, 2016, **45**, 217; (*b*) P. Sarkar, Z. Sun, T. Tokuhira, M. Kotani, S. Sato and H. Isobe, *ACS Cent. Sci.*, 2016, **2**, 740; (*c*) Y. Yang, Y. Nanjo, H. Isobe and S. Sato, *Org. Biomol. Chem.*, 2020, **18**, 4949; (*d*) T. Matsuno, Y. Yang, Y. Nanjo, H. Isobe, S. Sato, T. Matsuno, Y. Yang, Y. Nanjo, H. Isobe and S. Sato, *Chem. Lett.*, 2021, **50**, 110.
10 D. Lorbach, A. Keerthi, T. M. Figueira-Duarte, M. Baumgarten, M. Wagner and K. Müllen, *Angew. Chem., Int. Ed.*, 2016, **55**, 418.
11 K. Sato, M. Hasegawa, Y. Nojima, N. Hara, T. Nishiuchi, Y. Imai and Y. Mazaki, *Chem.–Eur. J.*, 2020, **26**, 1.
12 J. Nogami, Y. Tanaka, H. Sugiyama, H. Uekusa, A. Muranaka, M. Uchiyama and K. Tanaka, *J. Am. Chem. Soc.*, 2020, **142**, 9834.
13 K. Watanabe, Y. Segawa and K. Itami, *Chem. Commun.*, 2020, **56**, 15044.
14 For selected recent reviews, see: (*a*) Y. Shibata and K. Tanaka, Rhodium(I)-Catalyzed [2+2+2] and [4+2] Cycloadditions, in *Rhodium Catalysis in Organic Synthesis: Methods and Reactions*, ed. K. Tanaka, Wiley-VCH, Weinheim, 2019, p. 183; (*b*) K. Tanaka, *TCI Mail*, 2018, **179**, 3; (*c*) Y. Shibata and K. Tanaka, *Synthesis*, 2012, **44**, 32; (*d*) K. Tanaka, *Heterocycles*, 2012, **85**, 1017; (*e*) K. Tanaka, *Chem.–Asian J.*, 2009, **4**, 508; (*f*) K. Tanaka, *Synlett*, 2007, **18**, 1977.
15 For the enantioselective synthesis of a Möbius-shaped cycloparaphenylene, see: S. Nishigaki, Y. Shibata, A. Nakajima, H. Okajima, Y. Masumoto, T. Osawa, A. Muranaka, H. Sugiyama, A. Horikawa, H. Uekusa, H. Koshino, M. Uchiyama, A. Sakamoto and K. Tanaka, *J. Am. Chem. Soc.*, 2019, **141**, 14955.
16 Very recently, the stereoselective synthesis of two enantiomers of chiral conjugated nanohoops was reported. See:M. Hermann, D. Wassy, J. Kohn, P. Seitz, M. U. Betschart, S. Grimme and B. Esser, *Angew. Chem., Int. Ed.*, 2021, **60**, 10680.
17 H. Shimizu, I. Nagasaki and T. Saito, *Tetrahedron*, 2005, **61**, 5405.
18 (*a*) G. Naulet, L. Sturm, A. Robert, P. Dechambenoit, F. Röhricht, R. Herges, H. Bock and F. Durola, *Chem. Sci.*, 2018, **9**, 8930; (*b*) X. Jiang, S. D. Laffoon, D. Chen, S. Pérez-Estrada, A. S. Danis, J. Rodríguez-López, M. A. Garcia-Garibay, J. Zhu and J. S. Moore, *J. Am. Chem. Soc.*, 2020, **142**, 6493.
19 S. Kinoshita, R. Yamano, Y. Shibata, Y. Tanaka, K. Hanada, T. Matsumoto, K. Miyamoto, A. Muranaka, M. Uchiyama and K. Tanaka, *Angew. Chem., Int. Ed.*, 2020, **59**, 11020.
20 Y. Kimura, Y. Shibata, K. Noguchi and K. Tanaka, *Eur. J. Org. Chem.*, 2019, **2019**, 1390.
21 M. Gingras, G. Félix and R. Peresutti, *Chem. Soc. Rev.*, 2013, **42**, 1007.
22 P. Sehnal, I. G. Stará, D. Šaman, M. Tichý, J. Míšek, J. Cvačka, L. Rulíšek, J. Chocholoušová, J. Vacek, G. Goryl, M. Szymonski, I. Císařová and I. Starý, *Proc. Natl. Acad. Sci. U. S. A.*, 2009, **106**, 13169.
23 T. Matsushima, S. Kikkawa, I. Azumaya and S. Watanabe, *ChemistryOpen*, 2018, **7**, 278.
24 (*a*) H. Tanaka, Y. Inoue and T. Mori, *ChemPhotoChem*, 2018, **2**, 386; (*b*) H. Tanaka, M. Ikenosako, Y. Kato, M. Fujiki, Y. Inoue and T. Mori, *Commun. Chem.*, 2018, **1**, 38; (*c*) H. Kubo, D. Shimizu, T. Hirose and K. Matsuda, *Org. Lett.*, 2020, **22**, 9276.